Research on Engineering Structures & Materials
www.jresm.org
MIM Research Group

Research Article

Mechanical and microstructural evaluation of friction stir welded aluminum alloys under as-welded and heat-treated conditions

Dhanyashree P [*,a], N Nagesha [b]

Department of I&PE, University BDT College of Engineering, Davangere, India

Article Info

Article History:

Received 15 Feb 2026

Revised 15 June 2026

Keywords:

Friction stir welding;
Process parameters;
Heat treatment;
Mechanical properties;
Microstructure

Abstract

Enhancing the strength and reliability of aluminium alloy joints remains a key challenge in industrial applications. Combining alloys with complementary properties offers the potential to optimize weight, strength, and corrosion resistance; however, joining dissimilar aluminium alloys is inherently difficult. Differences in chemical composition, thermal conductivity, and precipitation behavior often lead to microstructural incompatibilities, making it challenging to produce high-quality, reliable joints. Friction stir welding (FSW) has emerged as a promising solid-state joining technique for aluminium alloys. This study investigates the effect of post-weld heat treatment (PWHT) on the mechanical properties, microstructure, and fracture behavior of friction stir welded dissimilar joints of AA6061-T6 and AA5052-H32 alloys. Microstructural analysis revealed fine equiaxed grains in the AW stir zone, which coarsened moderately post-treatment, accompanied by improved precipitate distribution. Mechanical testing showed that PWHT significantly improved joint performance, increasing the ultimate tensile strength from 196.14 MPa in the as-welded (AW) condition to 258.78 MPa, and enhancing joint efficiency to 32%. Fractographic analysis confirmed ductile fractures, and PWHT resulted in a more refined and uniformly distributed dimple morphology, as an indicative of enhanced plastic deformation capacity and improved fracture resistance. These results demonstrate that PWHT effectively mitigates localized softening, enhances ductility, and improves the structural integrity of dissimilar aluminium alloy FSW joints.

1. Introduction

Friction Stir Welding (FSW) is a solid-state joining technique pioneered in the early 1990s, has emerged as a transformative solution for welding both similar and dissimilar materials, particularly aluminum alloys. Unlike conventional fusion welding, FSW operates below the melting point, thereby minimizing defects such as porosity, hot cracking, and distortion [1–3]. This process has gained widespread adoption across aerospace, automotive, marine, electronics enclosure, medical, transportation, and structural engineering applications due to its ability to produce high-integrity joints with superior mechanical and corrosion-resistant properties [4,5].

Recent studies have demonstrated that the microstructural evolution and mechanical performance of FSW joints are highly sensitive to alloy composition, process parameters, and tool design. In particular, dissimilar welding of aluminum alloys presents unique challenges in achieving optimal material flow and interface bonding [6,7]. Understanding the interplay between thermal cycles, grain refinement, and precipitate behavior is crucial for tailoring joint properties to specific engineering applications. Kumar et al. [8] carried out a comprehensive review of FSW of 7075 aluminium alloy, emphasizing the influence of tool geometry, environmental parameters, and

*Corresponding author: dhanyashree.prabhakara@gmail.com
[a]orcid.org/0009-0002-0055-679X; [b]orcid.org/0000-0001-9088-1734
DOI: http://dx.doi.org/10.17515/resm2026-1511me0215rs

mathematical modelling on heat input, microstructural evolution, and mechanical performance. Feddal et al. [9] analyzed parameters and property relationships in FSW of aluminium alloys, detailing defect formation mechanisms and post-weld performance, including corrosion and fatigue behaviors. Threadgill et al. [10] delivered a foundational review of FSW in aluminium alloys, describing microstructural zones, hardness profiles, and mechanical property trends for heat-treatable and non-heat-treatable alloys.

Experimental studies have further advanced understanding of the relationship between process control, microstructure, and mechanical properties in FSW joints. Gibson et al. [11] discussed process automation, sensing, and control strategies, along with weld quality evaluation methods, providing a framework for systematic comparison of as-welded (AW) and post-heat-treated joints. Kumar et al. [12] examined dissimilar AA2024/AA6082 joints, showing that optimized process parameters enhanced both as-welded and heat-treated performance, thereby reinforcing the importance of parameter control in achieving desired joint properties.

A number of studies have examined how post-weld heat treatment affects the quality of dissimilar aluminum alloy friction stir welds on a systematic basis. Lakshminarayanan and Balasubramanian [13] showed that the use of optimized welding parameters together with post-weld heat treatment resulted in a significant improvement in both the tensile strength and the overall joint efficiency relative to the as-welded condition. In addition, Sato et al. [14] found that the microstructural recovery and redistribution of precipitates in AA6063 welded joints due to post-weld heat treatment restored hardness and increased ductility. Kumar and Kailas [15] also showed how axial load application followed by post-weld heat treatment positively affects tensile properties of 6061 dissimilar joints compared to the AW condition, with substantial increases in strength and elongation. Further, Elangovan and Balasubramanian [16] also showed that the use of post-weld heat treatment optimizes joint efficiency when used with an optimized tool geometry, offering comparative insights into microstructural stability and property changes after heat treatment.

Further, Abdel-Hamid I. Mourad and Mohamed Elwakil [17] studied the effect of Al_2O_3 particle volume fraction on the microstructure and mechanical properties of aluminum matrix composites prepared by friction stir processing (FSP), highlighting reinforcement, matrix interactions under severe plastic deformation. Advanced modelling approaches, such as hybrid LSTM–dense neural networks [18], have been applied to predict corrosion rates in friction stir welded flange joints, offering data-driven insights into long term durability. Comparative studies of FSW and TIG welding of AA3003 aluminum flange joints [19] under varying tool geometries and rotational speeds have clarified differences in heat input, defect susceptibility, and joint efficiency. Multi-response optimization frameworks combining RSM–ANN–GRA–TOPSIS [20] have been employed for AA6063-T6, demonstrating the potential of hybrid computational methods in parameter selection. Additionally, submerged friction stirs welding of AZ31C magnesium alloy [21] has been investigated to elucidate the effect of rotational speed on microstructural evolution and mechanical performance, underscoring the adaptability of FSW to non-aluminum systems.

While these studies collectively provide a robust understanding of FSW process parameters, microstructural evolution, and mechanical performance, there remains limited systematic comparison of as-welded and post-heat-treated aluminum alloy joints under identical processing conditions. Furthermore, the correlation between microstructural stability, grain refinement, and mechanical property retention in heat-treated FSW joints is not yet fully established. The present study addresses this gap by evaluating the mechanical and microstructural characteristics of friction stir welded AA6061-T6 and AA5052-H32 dissimilar joints in both as-welded and heat-treated conditions, with emphasis on quantifying the relationship between microstructural features and joint performance.

2. Experimental Procedure

The experimental workflow comprised material selection, definition of welding parameters, experimental setup, welding, and post-weld heat treatment.

2.1. Materials

The materials used in the present work are AA5052-H32 and AA6061-T6, cold rolled aluminum alloys. Table 1 and Table 2 show the composition and the mechanical characteristics of the base materials.

Table 1. Chemical composition of base materials - element (%by wt.)

Alloy	Si	Cu	Mn	Mg	Cr	Zn	Ti	Fe	Al
AA6061	0.45	0.21	0.10	0.925	0.110	0.013	0.013	0.31	Reminder
AA5052	0.13	0.01	0.02	2.31	0.17	0.01	-	0.34	Reminder

Table 2. Mechanical properties of base materials

Alloy	Ultimate Tensile Strength [UTS] (MPa)	Elongation (%)	Hardness (HV)
AA6061	313	9	105
AA5052	221	12	80

2.2. Welding Setup

FSW was carried out using an ETA Stir Welding Machine WS0002, a 3-axis system capable of delivering up to 100 kN axial thrust, with adjustable parameters to tailor high-quality joints. The two 6 mm aluminium plates to be welded were cut into 150 mm × 35 mm each. The surfaces were property cleaned using acetone to remove all dirt on the metal surface. The welding was performed along the rolling direction of the plates in butt configuration with AA6061-T6 on Advancing Side (AS), while 5052-H32 on Retreating Side (RS). The schematic representation of FSW process is given in Fig. 1 and 2, and the fixture, tool setup and joint configuration is shown in Fig. 3.

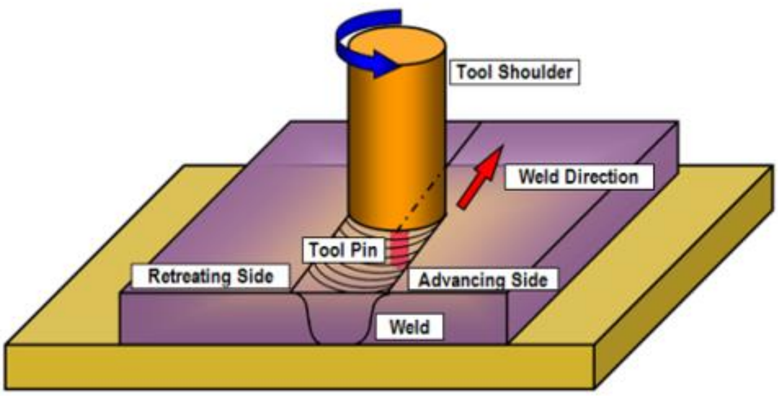

Fig. 1. Schematic of FSW process

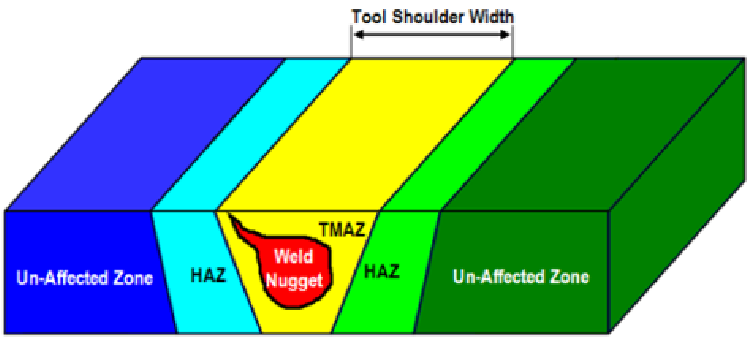

Fig. 2. Zones in a typical FSW butt joint

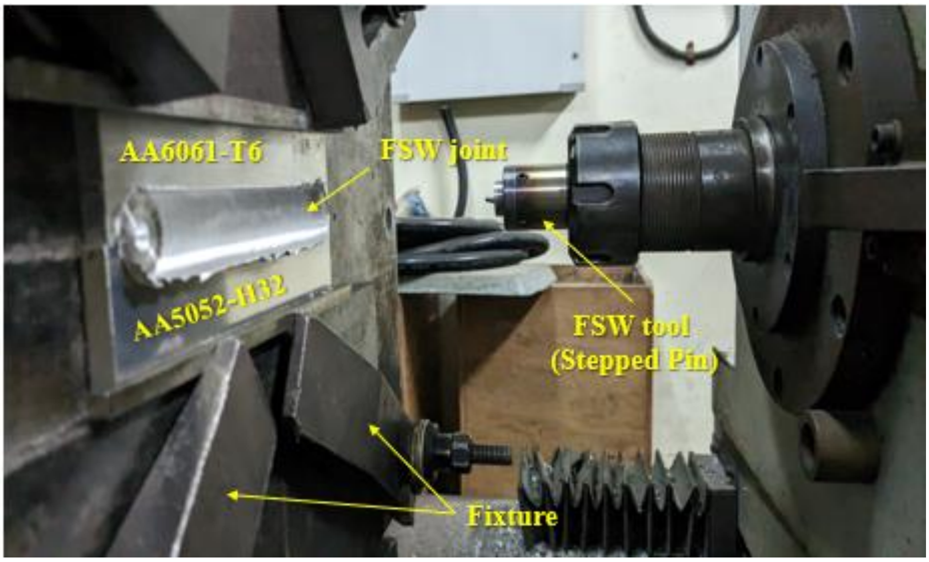

Fig. 3. FSW setup and butt welded sample

2.3. Process Parameters

Process parameter optimization in FSW is crucial for achieving defect-free joints with superior mechanical and metallurgical properties. The key controllable parameters, listed in Table 3, directly influence heat generation, material flow, and microstructural evolution within the weld zone. Excessive heat input due to high rotational speeds can lead to grain coarsening, whereas insufficient heat resulting from low rotational speeds or high welding speeds may cause void formation and incomplete bonding [22]. Therefore, an optimal balance among these parameters is essential to ensure adequate plasticization, mixing, and consolidation of the material. Recent work on multilayer multi-pass friction stir welding of dissimilar aluminium alloys has emphasized the importance of Taguchi's DOE and ANOVA in enhancing mechanical properties of complex weld configurations [23]. Hence, to identify the best combination of parameters for maximizing tensile strength, the Taguchi design of experiments has been employed in this study. Among the tested configurations, the joint produced using a tool rotational speed of 1000 rpm, a tool traverse speed of 40 mm/min, and a plunge depth of 5.77 mm with a stepped tool pin exhibited superior tensile behavior and is considered optimal.

Table 3. Process parameters

Parameter	Value
Tool rotational speed (RPM)	1000, 1200, 1400
Tool traverse speed (mm/min)	30, 40, 50
Plunge depth (mm)	5.6, 5.77, 5.94
Pin geometry	Cylindrical, Taper, Step
Tilt angle (∘)	0
Axial force (kN)	2
Dwell time (s)	10

2.4. Heat Treatment

The optimal joint specimen was sectioned transverse to the weld line in accordance with the ASTM E8 standard for tensile and hardness evaluation. Subsequently, the specimens were subjected to a post weld heat treatment to achieve the T6 temper condition and enhance mechanical performance. Solution heat treatment was carried out by heating the samples to 480 °C and holding for 3600 s to ensure complete dissolution of strengthening precipitates. Immediately after solution sing, the specimens were quenched in water at room temperature to retain a supersaturated solid solution. Artificial aging was then performed at 120 °C for 24 h, followed by air cooling to room temperature, thereby completing the T6 tempering cycle [24].

2.5. Testing and Analysis Methodology

To comprehensively evaluate the mechanical and microstructural performance of welded joint, a set of standardized tests and analyses were conducted. The methodology encompassed tensile testing, hardness profiling, and optical microstructural characterization, each designed to capture property variations across the weld zones and to assess the influence of post-weld heat treatment.

2.5.1. Tensile Testing

Micro-tensile specimens were extracted perpendicularly through the weld line using wire EDM, thereby preventing residual stresses and any changes in microstructure to capture the property gradations throughout the entire weld zone and base metal. The micro tensile specimens prior to testing and their dimensional details are shown in Fig. 4. Each of the specimens had a gauge length of 15 mm and thickness of 6 mm. Thus, all specimens were fabricated using ASTM standards (subsize option) and ISO standards (non-proportional) with elongation values given relative to their actual gauge lengths [25]. For each condition, three replicate micro-tensile specimens were fabricated and tested using the same Test Conditions, results of tensile testing are reported as mean values.

Tensile testing was completed for all specimens in both as welded and post welded heat-treated conditions using an X-Force P-type Zwick/Roell Z250 machine with a cross head speed of 1 mm/min, corresponding to a nominal strain rate of ±2×10^{-3} s^{-1}, in accordance with ASTM E8M-16a. All tests were conducted at room temperature (~25 °C).

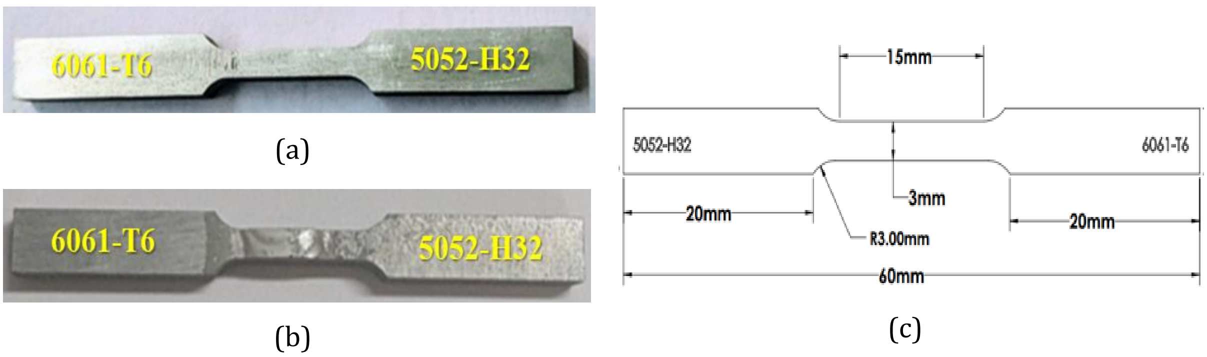

Fig. 4. Extracted micro-tensile specimens: AW specimen (b) PWHT specimen (c) Dimensional schematic

2.5.2. Hardness Testing

To further substantiate the mechanical performance of the joints, Micro-hardness testing using the Vicker method was conducted on weld cross-sections at various locations. The hardness testing was carried out in the various zones, making indentations at regular intervals using a 500 g load (HV 0.5) with 15 second dwell time on the welds for investigating the hardness of each weld cross section including base metals (BM), heat affected zones (HAZ), thermo-mechanical affected zones (TMAZ) and stir zone (SZ).

2.5.3. Microstructural Characterization

Microstructural study was carried out to examine grain morphology and phase distribution across the weld zone. Samples were sectioned from the welded joints, followed by standard metallographic preparation involving grinding with progressively finer silicon carbide papers and polishing using alumina suspension to achieve mirror-like surfaces. The polished specimens were examined under an Olympus optical microscope at 100× magnification to observe microstructural features.

2.5.3. Fractographic Analysis

To investigate the failure mechanisms of the tensile-tested specimens in both AW and PWHT conditions, fractographic examination was carried out using a Tescan Vega 3LMH Scanning Electron Microscope (SEM). All specimens were cleaned by ultrasonically cleaning in ethanol and mounted on conductive supports prior to imaging. The imaging was performed at 10 µm with a 15 kV, which provided sufficient detail to identify the characteristics of each fracture surface and to determine the mode of fracture.

3. Results and discussion

The following section presents the mechanical, hardness, microstructural, and fractographic findings for the friction stir welded joints and interprets these results in the context of welding condition and post-weld heat treatment.

3.1. Tensile Analysis

The tensile response of the dissimilar aluminium joints is presented here to highlight the comparative performance of the AW and PWHT conditions. The discussion focuses on strength levels, ductility trends, joint efficiency and fracture behavior, with representative stress–strain curves to illustrate the observed differences. The fractured specimens after testing are depicted in Fig. 5.

(a)

(b)

Fig. 5. Fractured micro-tensile specimens: FSW-AW specimen (b) PWHT specimen

The stress–strain behavior of the AW (Fig. 6) and PWHT (Fig. 7) specimens exhibited distinct differences in both strength and ductility. The AW specimen exhibited a steep initial elastic region, followed by yielding at a comparatively lower stress (yield strength of 112 MPa), and subsequently reached the UTS of 196.15 MPa before undergoing gradual necking and final fracture. This behavior reflects the combined influence of residual stresses, microstructural heterogeneity which together limit both load-bearing capacity and elongation in the as-welded condition [26,27].

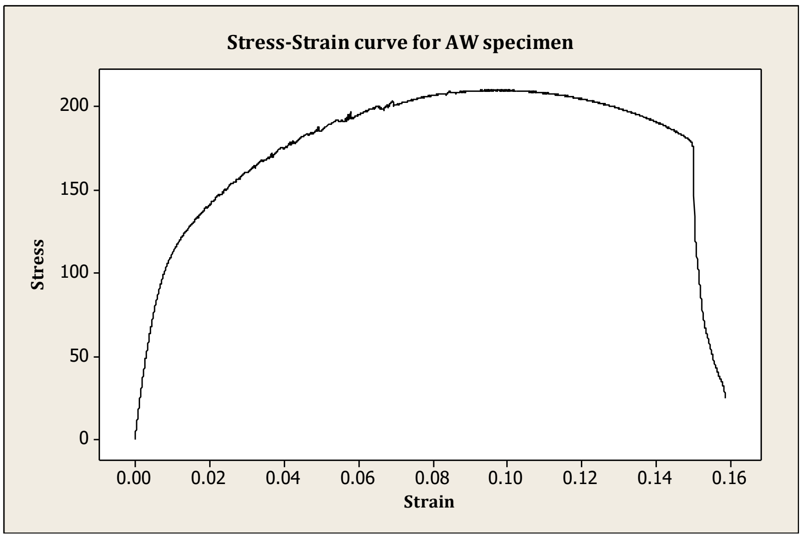

Fig. 6. Tensile behavior: AW specimen

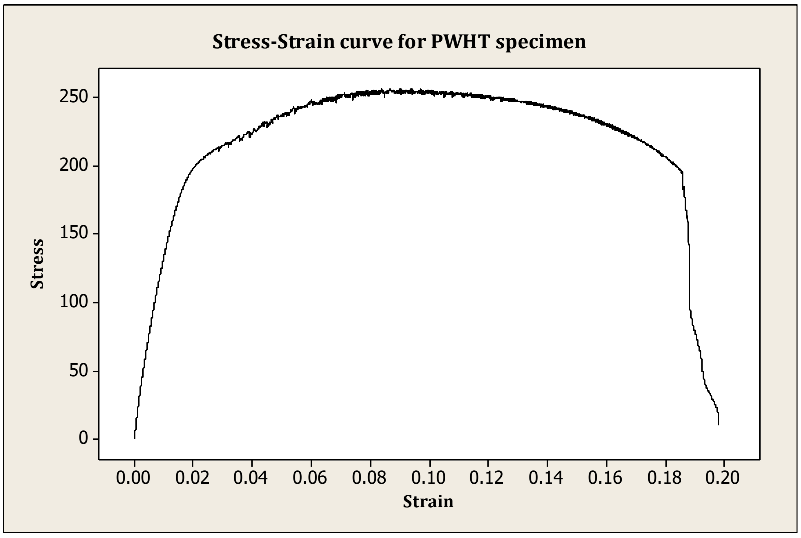

Fig. 7. Tensile behavior: PWHT specimen

In contrast, the PWHT specimen demonstrated a higher yield strength of 133 MPa and a significantly increased UTS of 258.78 MPa, accompanied by a broader plastic deformation region and greater total strain to fracture. The enhanced performance is attributed to the relief of residual stresses, homogenization of the weld microstructure, and reduction of brittle phases during heat treatment, which collectively improve both strength and ductility [28,29]. The smoother post UTS decline in the PWHT curve indicates more uniform necking and a predominantly ductile fracture mode compared to the AW condition.

3.1.1 Joint Efficiency

Joint efficiency is a widely used metric for evaluating the mechanical performance of welded joints relative to their base materials. It refers to how strong a welded joint is compared to the base material. It is calculated by comparing the UTS of the weld to that of the base metal and reporting this comparison as a percentage. This parameter provides a direct indication of how effectively the welding process has preserved or enhanced the inherent strength of the parent alloys and it is determined using below:

$$Joint\ efficiency\ (\%) = \frac{UTS_{joint}}{UTS_{BM}} \times 100 \quad (1)$$

Where, UTS_{joint}: Ultimate Tensile Strength of welded joint, UTS_{BM}: Ultimate Tensile Strength of base material.

Table 4. Joint efficiency of AW and PWHT specimens relative to base materials

Specimen	Reference	BM UTS (MPa)	Joint UTS (MPa)	Efficiency (%)
AW	stronger BM (AA6061-T6)	314	196.15	(196.15/314) x 100 = 62.45
AW	weaker BM (AA5052-H32)	218	196.15	(196.15/218) x 100 = 89.98
PWHT	stronger BM (AA6061-T6)	314	258.78	(258.78/314) x 100 = 82.41
PWHT	weaker BM (AA5052-H32)	218	258.78	(258.78/218) x 100 = 118.70

The UTS of welded joints was measured to be 196 MPa in AW condition, that equates to 62.45% of the UTS of the stronger AA6061-T6 material and 89.98% of the weaker AA5052-H32 material. Although the UTS of the welded joint is significantly lower than the AA6061-T6 alloy, the efficiencies of the weld joint are still considerable, relative to both AW and AA5052-H32 alloy. Further, the UTS of PWHT joint resulted in 259 MPa. This results in joint efficiencies of 82.41% and

118.70% compared to the AA6061-T6 and AA5052-H32 materials, respectively. The efficiency greater than 100% indicates that the weld joint area is now stronger than the AA5052-H32 alloy as a result of grain size refinement and precipitation hardening. This refers to the increased efficiency and mechanical performance of the PWHT welded joint compared to AW joint based on its capacity to retain the foundational strengths of the weaker alloy. This result demonstrates that the beneficial effects of heat treatment towards closing the gap between the strength of the joint and the strength of the AA6061-T6 base material and increasing the weld zone performance beyond that of the AA5052-H32 base material. Hardness mapping across the weld cross-sections shown in Fig. 9 provided insight into localized property variations induced by welding and subsequent heat treatment. The results emphasize zone-wise differences in hardness and the extent to which PWHT mitigates gradients, thereby supporting the interpretation of tensile performance.

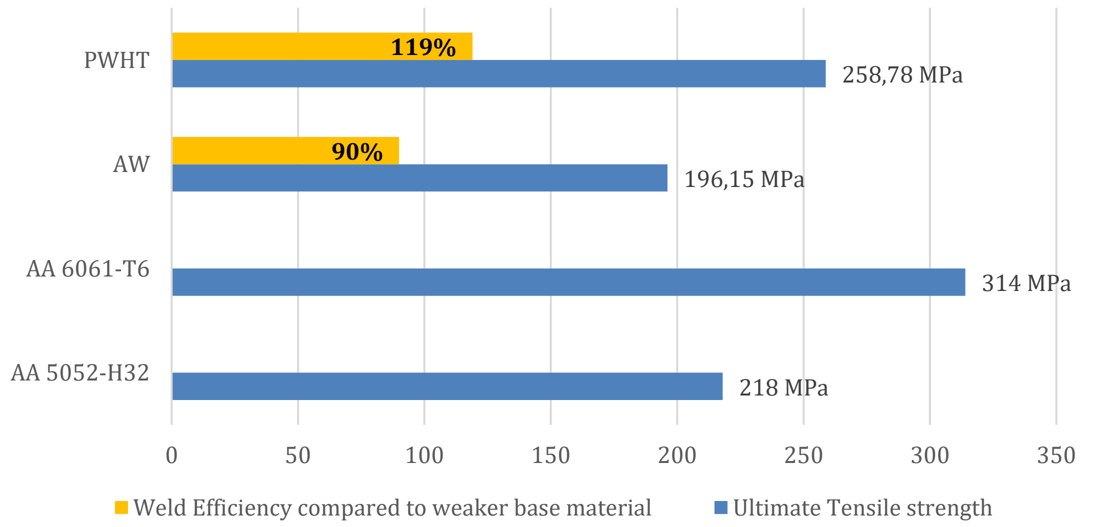

Fig. 8. Joint efficiency comparison

$$Improvement\ from\ AW\ to\ PWHT = \frac{UTS_{PWHT} - UTS_{AW}}{UTS_{AW}} \times 100 \quad (2)$$

$$= \frac{258.78 - 196315}{196.15} \times 100 = \mathit{31.94\%\ increase\ in\ UTS}$$

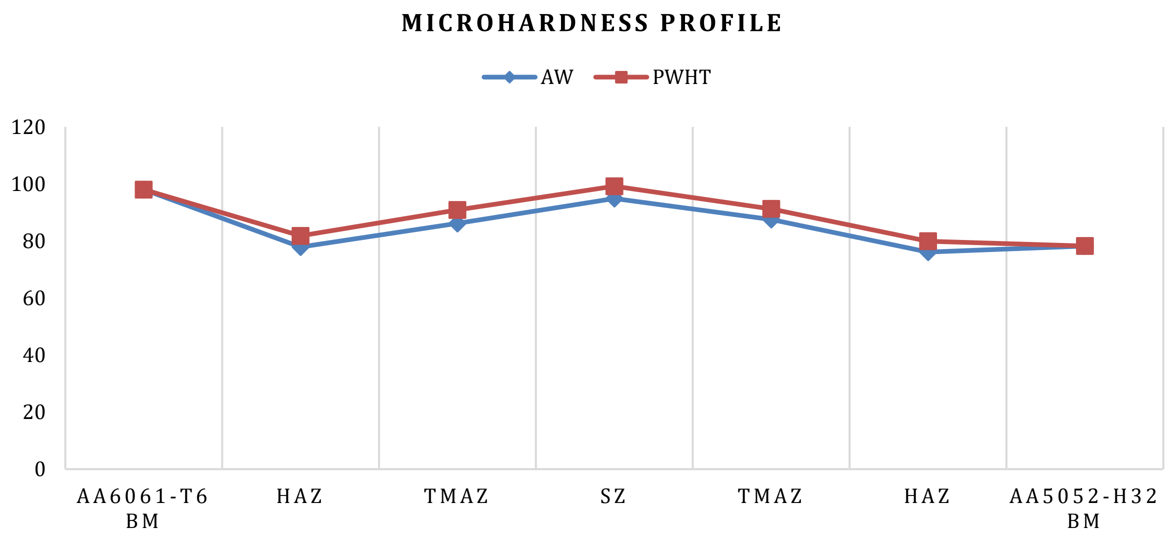

Fig. 9. Comparative microhardness profiles across weld zones for AW and PWHT joints

The micro-hardness distribution across the weld cross-section revealed distinct differences between AW and PWHT conditions. In the AW state, the stir zone exhibited a hardness of 94.89 HV, lower than the AA6061-T6 base metal due to dissolution and coarsening of Mg_2Si precipitates, while the HAZ on the AA6061-T6 side showed pronounced softening to 77.89 HV from precipitate over-aging. The AA5052-H32 side maintained relatively stable hardness, though reductions were observed in the HAZ (76.11 HV) and TMAZ (87.54 HV) owing to recovery of strain-hardening. After PWHT, hardness values increased across all zones, with the stir zone reaching 99.19 HV and the TMAZ recovering to ~91 HV, reflecting re-precipitation of fine Mg_2Si particles in AA6061-T6 and partial recrystallisation in AA5052-H32. The HAZ hardness also improved on both sides (81.79 HV in AA6061 and 79.91 HV in AA5052), thereby reducing the steep gradients observed in the AW condition. Overall, the hardness profiles confirm that PWHT mitigates localized softening, restores precipitate strengthening, and produces a more homogeneous distribution across the weld, consistent with the enhanced tensile strength and ductility observed in mechanical testing.

3.3. Microstructure Analysis

Optical microscopy results are presented to reveal grain morphology and phase distribution across the weld zones. The discussion connects microstructural features such as grain refinement, recrystallization, and phase transformations with the mechanical properties, offering a direct link between structure and performance.

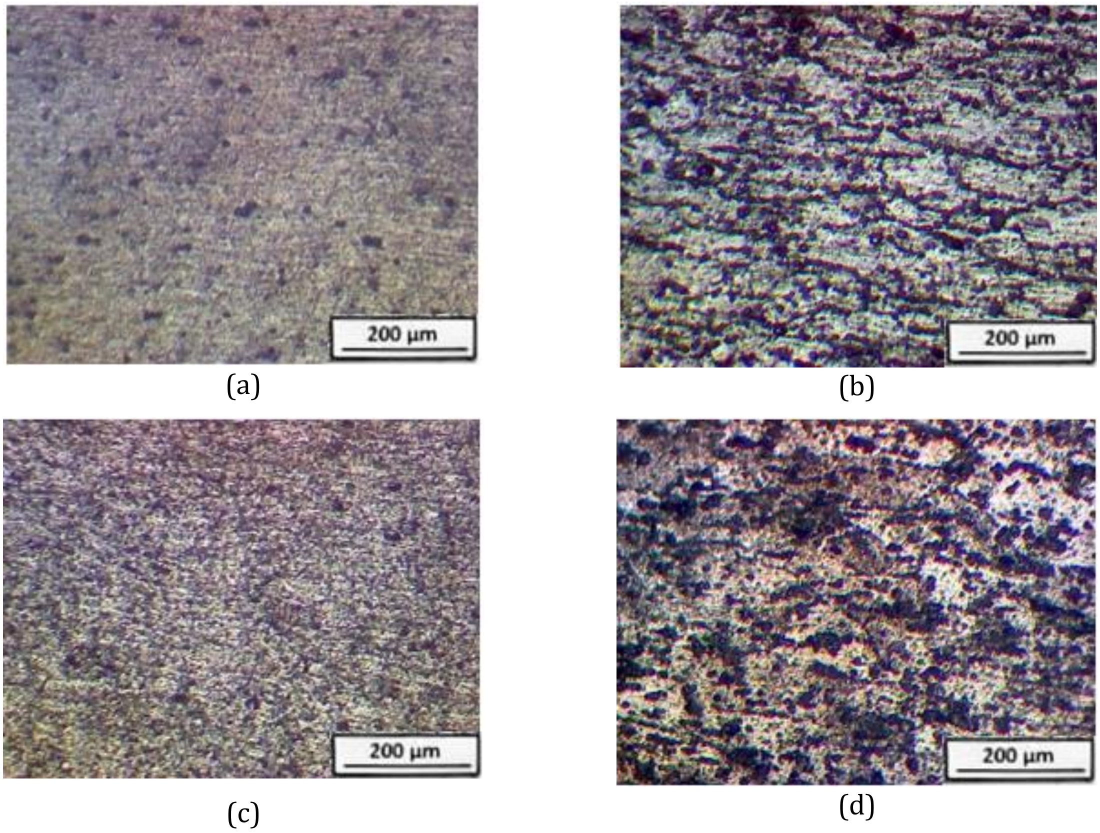

Fig. 10. Optical microstructure of base metal: (a) 6061-T6 as rolled (b) 6061-T6 as heat treated (c) 5052-H32 as rolled (d) 5052-H32 as heat treated

The AA6061-T6 base metal exhibits a fine, equiaxed α-Al grain structure typical of a precipitation hardened Al-Mg-Si alloy in the T6 temper, with uniformly distributed Mg_2Si precipitates and dispersoids contributing to high strength. Grain boundaries are well defined, with minimal signs of recovery or recrystallisation. In contrast, the AA5052-H32 base metal shows elongated, slightly deformed grains aligned with the rolling direction, characteristic of a strain-hardened, non-heat-treatable Al–Mg alloy. Strengthening arises from solid-solution hardening by magnesium and retained work-hardening, with fine dispersoids and occasional intermetallic particles present [30-32].

Table 5. Grain Morphology Comparison in FSW Zones

Zone	AW Condition	PWHT Condition
SZ	Fine grains from complete dynamic recrystallisation, uniform grain size in AA6061-T6; partial dissolution and coarsening of Mg_2Si precipitates in AA5052-H32; precipitate-free solid-solution matrix. 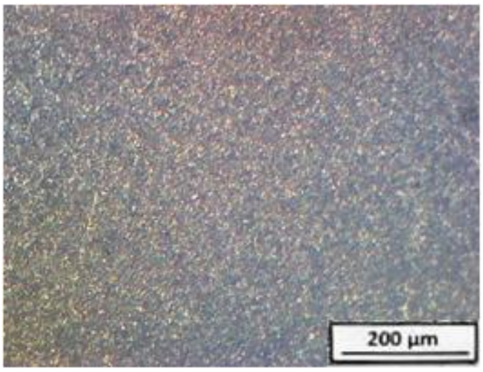	Equiaxed grains retained but moderately coarsened; in AA6061-T6, fine, uniformly re-precipitated Mg_2Si particles restore strength; in AA5052-H32, recovery and partial recrystallisation improve ductility. 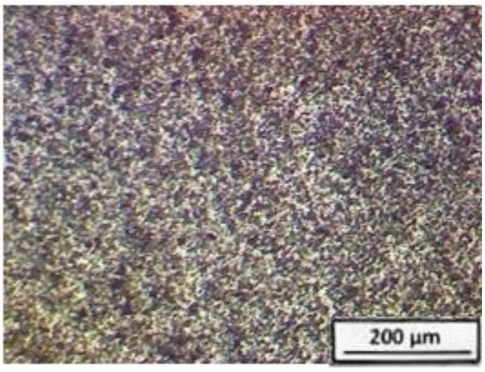
TMAZ	Elongated, deformed grains aligned with material flow, partial recrystallisation, precipitate coarsening in AA6061-T6; reduced dislocation density in AA5052-H32. 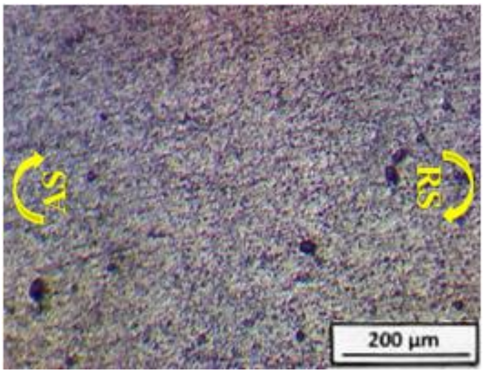	More equiaxed grains due to static recrystallisation, reduced deformation texture, precipitate distribution more uniform in AA6061-T6; further recovery in AA5052-H32. 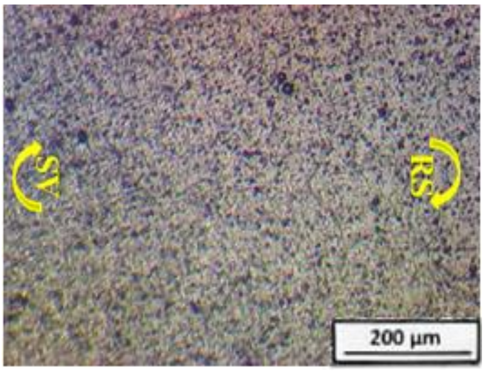
HAZ	Slightly coarser grains than BM, no deformation, over-aging and precipitate coarsening in AA6061-T6; recovery in AA5052-H32. 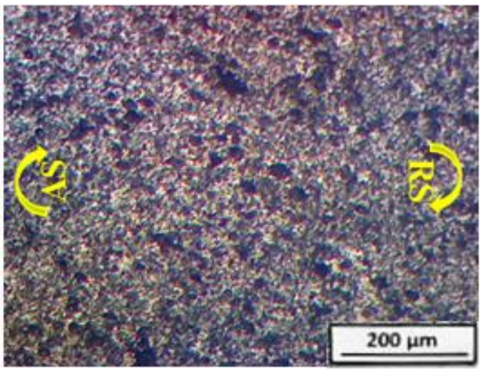	More homogeneous grain size, fine and uniformly distributed precipitates in AA6061-T6; partial recrystallisation in AA5052-H32; reduced hardness gradient. 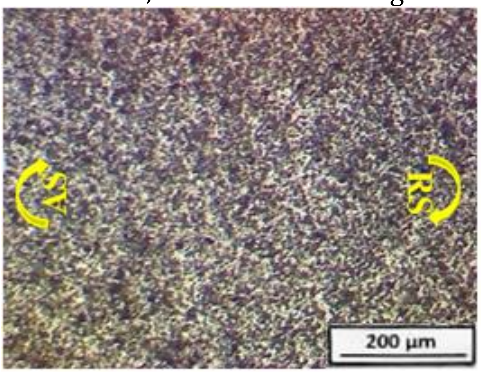

The generalized cross-sectional profile of a friction stir welded (FSW) joint can be described as an inverted trapezoid comprising four distinct microstructural zones: Stir Zone (SZ), Thermo-Mechanically Affected Zone (TMAZ), Heat-Affected Zone (HAZ), and Base Metal (BM), as shown in Fig. 2 [26,27]. The NZ, located beneath the tool shoulder and pin, experiences intense plastic deformation and elevated temperatures, producing fully recrystallized, fine equiaxed grains. The adjacent TMAZ undergoes both deformation and heating but without complete recrystallisation, resulting in elongated, deformed grains. The HAZ is influenced only by the thermal cycle, leading to grain or precipitate coarsening without plastic deformation. The BM retains its original grain structure and properties, remaining unaffected by the welding process [28,29]. After PWHT, AA6061-T6 shows partial recrystallisation, moderate grain coarsening, and a more uniform distribution of Mg_2Si precipitates, indicating homogenization and stress relief that enhance ductility while maintaining strength. Heat-treated AA5052-H32 displays reduced deformation texture and more equiaxed grains due to recovery and partial recrystallisation, relieving internal stresses but reducing strain hardening. While dispersoid distribution remains largely unchanged, annealing induced softening explains the potential hardness reduction on the 5052 side. Table 5 shows the microstructural comparison across all zones for both AS and PWHT conditions.

In addition, grain size was quantified per ASTM E112 using the linear intercept method. In the AW condition, the stir zone exhibits fine equiaxed grains (~8 μm, ASTM 9) formed through dynamic recrystallisation, which directly enhances hardness. By contrast, PWHT induces partial recrystallisation and moderate grain coarsening (~12–15 μm, ASTM 8). Although grains become slightly larger, PWHT promotes homogenization and re-precipitation of strengthening phases such as Mg_2Si, reduces residual stresses, and improves ductility. Thus, AW hardness is primarily governed by grain refinement, while PWHT mechanical performance arises from precipitate redistribution and stress relief, ensuring balanced strength and toughness across the weld. The microstructural observations indicate that PWHT improved the microstructural balance across all weld zones by promoting recovery, recrystallisation, and precipitate redistribution. These changes reduced heterogeneity between zones, mitigated hardness gradients, and contributed directly to the observed enhancement in UTS and joint efficiency. Thus, microstructural analysis confirms that PWHT is an effective route to strengthen dissimilar aluminium friction stir welds while improving ductility and structural reliability.

3.3. Fracture Morphology

The SEM fractography of fractured specimens are reviewed in order to identify the primary mechanisms by which the specimens failed when subjected to AW and PWHT conditions. The examination revealed several key characteristics of the failed areas. Understanding these characteristics helps to identify the fractures' failure modes with respect to how microstructural changes impact the fracture behavior.

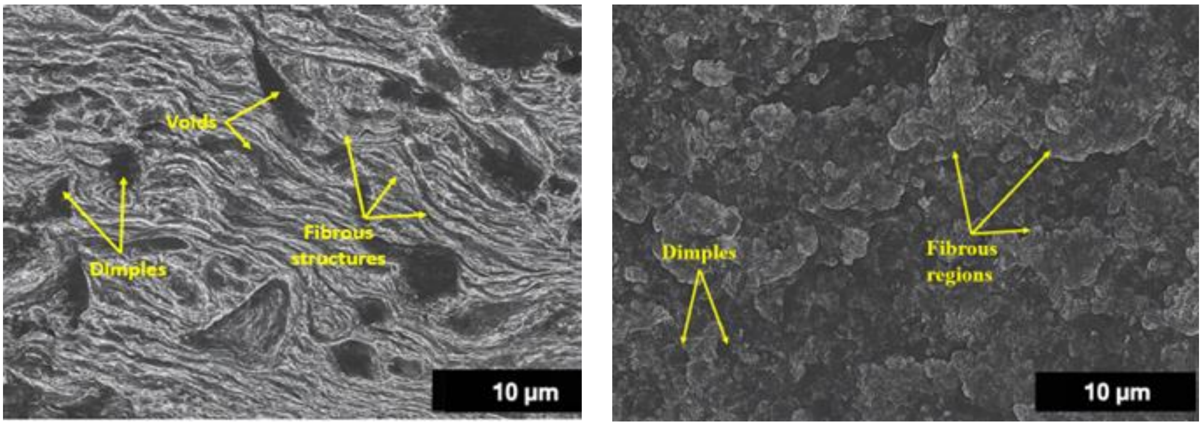

(a) (b)

Fig. 11. Fractographic images (a) AW tensile sample (b) PWHT tensile sample

In the AW condition, fracture occurred on the AA5052-H32 side within the softened HAZ and TMAZ. Macroscopically, specimens showed pronounced necking with shear lips, while SEM revealed predominantly ductile fracture with large, equiaxed dimples formed by micro-void coalescence. Voids nucleated at intermetallic particles and dispersoids, then grew and coalesced under tensile loading. Crack initiation occurred at particle matrix interfaces in the HAZ, propagating through the TMAZ until final rupture. Fig. 11 shows the SEM images of AW and PWHT fractured specimens.

In PWHT condition, fracture remained on the AA5052-H32 side but with more uniform necking and a path closer to the nugget zone when HAZ hardness recovery was significant. SEM showed deeper, more uniformly distributed dimples, reflecting improved ductility from recovery and partial recrystallisation, along with reduced void density at coarse particles. These observations align with tensile results, where AW joints exhibited lower UTS and elongation due to localized softening, while PWHT joints demonstrated improved strength and ductility. In both conditions, the fracture mode was predominantly ductile, confirming that failure was governed by localized softening rather than brittle mechanisms.

4. Conclusions

The present investigation examined dissimilar friction stir welded joints of AA6061-T6 and AA5052-H32 under AW and PWHT conditions, with emphasis on correlating mechanical performance, microstructural evolution, hardness distribution, and fracture morphology. The important conclusions drawn from this study are:

- Mechanical testing results demonstrated that AW joints exhibited reduced strength due to microstructural heterogeneity and localized softening. UTS of the AW condition was 196.15 MPa, corresponding to joint efficiencies of 62.45% relative to AA6061-T6 and 89.98% relative to AA5052-H32. In contrast, PWHT significantly improved mechanical performance, raising UTS to 258.78 MPa and joint efficiencies to 82.41% and 118.70%, respectively. This improvement represents a 31.94% increase in strength, confirming that heat treatment is an effective route to enhance the load-bearing capacity of dissimilar friction stir welds.
- Hardness measurements substantiated these observations. The AW condition showed pronounced softening in the HAZ of AA6061-T6, while the stir zone hardness was slightly lower than the base metal. PWHT improved hardness values across all zones, particularly in the stir zone and TMAZ, and reduced steep gradients between weld zones and base metals. This homogenization of hardness distribution directly supports the enhanced tensile strength and ductility observed in mechanical testing.
- Microstructural characterization revealed clear differences between AW and PWHT conditions. In the AW state, the SZ contained fine equiaxed grains formed by dynamic recrystallisation, while the TMAZ exhibited elongated grains and the HAZ showed grain coarsening and precipitate over-aging. After PWHT, the stir zone retained equiaxed grains with moderate coarsening, but re-precipitation of fine Mg_2Si particles in AA6061-T6 restored strength. The AA5052-H32 side benefited from recovery and partial recrystallisation, which improved ductility. These changes reduced heterogeneity between zones and produced a more balanced microstructure across the weld.
- Fractographic analysis confirmed that fracture in both AW and PWHT conditions occurred on the AA5052-H32 side and was predominantly ductile. AW specimens showed larger dimples and localized softening, while PWHT specimens exhibited deeper, more uniformly distributed dimples and more homogeneous necking, reflecting improved ductility and reduced void density.

In summary, PWHT enhanced strength, ductility, and joint efficiency by stabilizing microstructure, redistributing precipitates, and mitigating hardness gradients. These improvements confirm that post-weld heat treatment is a reliable and effective strategy for strengthening dissimilar AA6061-T6/AA5052-H32 friction stir welds, making them more suitable for demanding structural applications where both strength and reliability are critical.

Acknowledgement

The authors gratefully acknowledge the Indian Institute of Science (IISc), Bengaluru, for providing the experimental facilities and technical support required to carry out this research.

References

[1] Mallieswaran K, Agaramudhalvan S, George Oliver D. Microstructural stability and strength correlation in AGG affected friction stir welded AA2024 T4 joints. Advances in Materials and Processing Technologies, 2025. https://doi.org/10.1080/2374068X.2025.2501044

[2] Kah P, Rajan R, Martikainen J, Suoranta R. Investigation of weld defects in friction stir welding and fusion welding of aluminium alloys. International Journal of Mechanical and Materials Engineering, 2015; 10: 26. https://doi.org/10.1186/s40712-015-0053-8

[3] Habba MIA, Ahmed MMZ. Friction stir welding based technologies: A comprehensive review from the sustainable manufacturing perspectives. Journal of Materials Research and Technology, 2025; 38: 1-29. https://doi.org/10.1016/j.jmrt.2025.07.184

[4] Patnaik S, Chattopadhyaya S, Shankar S. Friction stir welding and its applications: An overview. AIP Conference Proceedings, 2022; 2681: 020018. https://doi.org/10.1063/5.0116234

[5] Padhy GK, Wu CS, Gao S. Friction stir based welding and processing technologies - processes, parameters, microstructures and applications: A review. Journal of Materials Science & Technology, 2018; 34(1): 1-38. https://doi.org/10.1016/j.jmst.2017.11.029

[6] Liu H, Wu C, Xie R, Pan R, Chen X, Lin J, Chen S. Interface optimization design and bonding mechanism of friction rolling additive manufactured aluminum/steel dissimilar metal. Journal of Manufacturing Processes, 2024. https://doi.org/10.1016/j.jmapro.2024.11.040

[7] Kumar R, Lakshmikanthan A, Sharma P, Nikhade SD. A critical review of material flow investigation in friction stir welding using novel techniques. Materials and Manufacturing Processes, 2025; 40(16): 1663-1694. https://doi.org/10.1080/01694243.2025.2470256

[8] Kumar A, Gahlot P, Kumar A, Phanden RK. A state of the art literature review on friction stir welding of 7075 aluminium alloy. International Journal on Interactive Design and Manufacturing, 2024.

[9] Feddal I, Chairi M, Di Bella G. Analysis of friction stir welding of aluminum alloys. Metals, 2025; 15(5): 532. https://doi.org/10.3390/met15050532

[10] Threadgill PL, Leonard AJ, Shercliff HR, Withers PJ. Friction stir welding of aluminium alloys. International Materials Reviews, 2009; 54(2): 49-93. https://doi.org/10.1179/174328009X411136

[11] Gibson BT, Lammlein DH, Prater TJ, Longhurst WR, Cox CD, Ballun MC, Dharmaraj KJ, Cook GE, Strauss AM. Friction stir welding: Process, automation, and control. Journal of Manufacturing Processes, 2014; 16(1): 56-73. https://doi.org/10.1016/j.jmapro.2013.04.002

[12] Kumar R, Abdellah N, Kant N, Singh P, Hashmi AW, Malla C. Effect of FSW process parameters on mechanical properties and microstructure of dissimilar welded joints of AA2024 and AA6082. Materials Today: Proceedings, 2021; 50. https://doi.org/10.1016/j.matpr.2021.09.007

[13] Lakshminarayanan AK, Balasubramanian V. Process parameters optimization for friction stir welding of RDE-40 aluminium alloy using Taguchi technique. Materials and Design, 2008; 29(7): 1229-1241. https://doi.org/10.1016/S1003-6326(08)60096-5

[14] Sato YS, Urata M, Kokawa H. Microstructural evolution of 6063 aluminum during friction stir welding and its effect on mechanical properties. Metallurgical and Materials Transactions A, 2002; 33(3): 625-635. https://doi.org/10.1007/s11661-002-0124-3

[15] Kumar K, Kailas SV. On the role of axial load and post-weld heat treatment on tensile properties of friction stir welded AA6061. Materials Science and Engineering A, 2008; 485(1-2): 367-374. https://doi.org/10.1016/j.msea.2007.08.013

[16] Elangovan K, Balasubramanian V. Influence of tool pin profile and PWHT on tensile strength of friction stir welded AA6061 aluminum alloy. Materials and Design, 2008; 29(7): 1359-1366. https://doi.org/10.1016/j.matdes.2007.01.030

[17] Mourad AH, Elwakil M. Effect of Al_2O_3 particle volume fraction on the microstructure and mechanical properties of aluminum matrix composites prepared by friction stir processing. 2025.

[18] Sabry I, Mourad AH, Elwakil M. Hybrid LSTM-dense neural network for accurate corrosion rate prediction in friction stir welded flange joints. Engineering Applications of Artificial Intelligence, 2026; 167: 113697. https://doi.org/10.1016/j.engappai.2025.113697

[19] Sabry I, El Zathry NE, Mahamood RM, Akinlabi S, Woo WL. Comparative study of FSW and TIG welding of AA3003 aluminium flange joints under varying tool geometries and rotational speeds. Welding in the World, 2026; 70: 763-780. https://doi.org/10.1007/s40194-026-02352-y

[20] Sabry I, Mourad AH, Elwakil M. Multi response optimization of friction stir welding parameters for AA6063 T6 using hybrid RSM-ANN-GRA-TOPSIS. Materials Today Communications, 2026; 51: 114524. https://doi.org/10.1016/j.mtcomm.2025.114524

[21] Sabry I, Naseri M, Mourad AH. Elucidating the effect of rotational speed on submerged friction stir welding of AZ31C magnesium alloy. Journal of Materials Research and Technology, 2025; 39: 1080-1090. https://doi.org/10.1016/j.jmrt.2025.09.175

[22] Su Y, Zhou M, Li W, Yang X, Shi Q, Xiong Y, Wang P, Chen G. Microstructural evolution and mechanical behavior of TA5 titanium alloy joint in low temperature friction stir welding with various cooling rates. Engineering Failure Analysis, 2025; 159: 109667. https://doi.org/10.1016/j.engfailanal.2025.109667
[23] Chandrakumar C, Sogalad I, Shettigar AK, Korgal A, Nagaral M. Exploring welding parameter effects on friction stir weld joints in aluminum 8006 alloy using response surface methodology. Research in Engineering Structures and Materials, 2025; 11(4): 1561-1578.
[24] Lumley RN. Heat treatment of aluminum Alloys. In: Encyclopedia of Thermal Stresses. Springer, Dordrecht, 2014. https://doi.org/10.1007/978-94-007-2739-7_431
[25] Zhang L, Harrison W, Yar MA, Brown SGR, Lavery N. The development of miniature tensile specimens with non standard aspect and slimness ratios for rapid alloy prototyping processes. Journal of Materials Research and Technology, 2021; 15: 3623-3635. https://doi.org/10.1016/j.jmrt.2021.09.029
[26] Ashok P, Dhanalakshmi S, Sundararaj P. Friction stir welding of AA5052 and AA6061 aluminium alloy by using Taguchi method. International Research Journal of Engineering and Technology, 2019; 6(3): 1866-1872.
[27] Imam M, Racherla V, Biswas K, Fujii H, Chintapenta V, Sun Y, Morisada Y. Microstructure property relation and evolution in friction stir welding of naturally aged 6063 aluminium alloy. International Journal of Advanced Manufacturing Technology, 2017; 91: 1753-1769. https://doi.org/10.1007/s00170-016-9865-9
[28] Hassan AS, Mahmoud TS, Mahmoud FH, Khalifa TA. Corrosion behaviour of dissimilar A319 and A356 cast aluminum alloys joined by friction stir welding. Proceedings of the World Congress on Engineering, London, UK, 2010; Vol II. https://doi.org/10.1179/136217110X12720264008358
[29] Rao CM, Mallikarjuna Rao K. Evolution of microstructure and hardness of aluminium 6061 after friction stir welding. International Journal of Theoretical and Applied Mechanics, 2017; 12(3): 405-410.
[30] Senthamaraikannan B, Krishnamoorthy J. Material flow and mechanical properties of friction stir welded AA5052 H32 and AA6061 T6 alloys with Sc interlayer. Materials Testing, 2023; 65(7): 1127-1142. https://doi.org/10.1515/mt-2022-0352
[31] Lee WB, Yeon YM, Jung SB. The joint properties of dissimilar formed Al alloys by friction stir welding according to the fixed location of materials. Scripta Materialia, 2004; 51(9): 863-868.
[32] Bhushan RK, Sharma D. Investigation of mechanical properties and surface roughness of friction stir welded AA6061 T651. International Journal of Mechanical and Materials Engineering, 2020; 15(7): 1-14. https://doi.org/10.1186/s40712-020-00119-x
[33] ASTM International. Standard Test Methods for Tension Testing of Metallic Materials (Designation: E8/E8M–13a). ASTM International, West Conshohocken, PA, USA, 2013. Approved as an American Association State Highway and Transportation Officials Standard (AASHTO No.: T68) and recognized as an American National Standard.
[34] Thomas, W.M., Nicholas, E.D., Needham, J.C., Murch, M.G., Temple-Smith, P., and Dawes, C.J. Friction Stir Welding Handbook. The Welding Institute (TWI), Cambridge, UK, 2001.
[35] Mishra, R.S., and Mahoney, M.W. *Friction Stir Welding and Processing.* ASM International, Materials Park, Ohio, USA, 2007.